CeraMetal: A New Approach to Low-Cost Metal 3D Printing with Bronze Clay

Leah Buechley
buechley@unm.edu
Department of Computer Science
University of New Mexico
Albuquerque, New Mexico, USA

Jaime Gould
egould@unm.edu
Department of Computer Science
University of New Mexico
Albuquerque, New Mexico, USA

Fiona Bell
fbell1@unm.edu
Department of Computer Science
University of New Mexico
Albuquerque, New Mexico, USA

Figure 1: A collection of metal objects 3D printed from our custom bronze clay including gears, a wrench, and jewelry.

ABSTRACT

This paper introduces CeraMetal, a low-cost and robust approach to desktop metal 3D printing based on a custom "metal clay". We present three recipes for 3D printable bronze clay along with a workflow that includes print parameters and a sintering schedule. We introduce custom slicing software that generates continuous extrusion toolpaths for metal clay printing. We analyze the shrinkage, density, tensile strength and flexibility of prints produced with Cerametal and find the material's performance comparable to parts produced via other bronze 3D printing methods. Finally, we provide several examples of 3D printed metal objects and a discussion of limitations and future research opportunities.

CCS CONCEPTS

• **Human-centered computing** → **Interactive systems and tools**; • **Applied computing** → **Computer-aided design**.

CHI '24, May 11–16, 2024, Honolulu, HI, USA

ACM ISBN 979-8-4007-0330-0/24/05
https://doi.org/10.1145/3613904.3642155

KEYWORDS

Digital Fabrication, 3D Printing, Metal 3D Printing, Metal Clay, Slicing Software, Toolpaths

ACM Reference Format:
Leah Buechley, Jaime Gould, and Fiona Bell. 2024. CeraMetal: A New Approach to Low-Cost Metal 3D Printing with Bronze Clay. In *Proceedings of the CHI Conference on Human Factors in Computing Systems (CHI '24), May 11–16, 2024, Honolulu, HI, USA.* ACM, New York, NY, USA, 16 pages. https://doi.org/10.1145/3613904.3642155

1 INTRODUCTION

The ability to 3D print in metal provides unique design, prototyping, and small-scale production opportunities. Metal 3D printing allows for the creation of durable metal parts that can be used in a range of applications in which plastic 3D printed parts are not suitable. Mechanical components like gears, cams, and linkages—capable of withstanding long-term real-world use–can be quickly designed and deployed. Artifacts traditionally made from metal, like jewelry and tableware, can be prototyped and manufactured in small to medium scales out of safe, functional, and beautiful materials.

Metal 3D printing has all of the rich affordances of traditional 3D printing, including the ability to create mathematically precise parts and the ability to create novel artifacts through computational design workflows. The direct production process, which does not require the creation of molds, is fast and flexible and facilitates iterative design. Printing does not require the mold making expertise required to employ traditional metal working techniques like lost-wax casting [57]. Printing is also less wasteful than either

Printing Method	**Material**	**Printer Cost**	**Kiln/Other Cost**	**Material Cost** $/kg	**Easily Recyclable**
Selective Laser Sintering [62]	Custom Powder	$130,000+	$50,000 Powder station	$ 45.00*	unclear
Bound Metal Deposition [89]	Custom Filament	$50,000+	$60,000 Furnace	unavailable	no
Fused Filament Fabrication [34]	Bronze Filamet™	$250+	$1000 Kiln	$ 225.00	no
CeraMetal	*Bronze powder*	*$700+*	*$1000 Kiln*	*$44.00*	*yes*

Table 1: Comparison of metal 3D printing technologies. Showing the least expensive current option in each category. *Must be purchased in bulk with a minimum order of ≈ $1300 [62].

mold-making and casting or subtractive processes like milling. To 3D print a metal part, one needs only the material that goes into the part. Material that would be used to create positive models and molds or material that would be milled away is not wasted. The compelling affordances of metal 3D printing have made it an important digital fabrication process. Unfortunately, it has long been an expensive and inaccessible one.

Most research and technology development in metal 3D printing has taken place in the context of manufacturing or mechanical engineering. The goal has been to develop materials and machines suitable for either industrial production [37, 72] or highly specialized application areas like aerospace [66] and internal medicine [54]. The most common metal printers, which work through a Selective Laser Sintering (SLS) process in which metal powder is sintered together with a laser, cost hundreds of thousands of dollars and require large amounts of expensive metal powder to operate [37]. Printed metal parts can be ordered through printing services like Shapeways[1], but even small parts can cost hundreds to thousands of dollars, and workflows that depend on 3D printing services are slow and cumbersome. More recently, it has become possible to take a Fused Filament Fabrication (FFF) approach to metal 3D printing [34, 60, 85], however, the custom metal filaments are still very costly.

As Human-Computer Interaction (HCI) researchers, we wanted to take a different approach, by developing inexpensive and easy-to-use technologies and techniques to enable researchers (and others) to experiment with metal printing in everyday contexts. We introduce a new approach to low-cost metal printing on the desktop that was inspired by the commercial availability of metal clays for jewelry [31, 77] and small, low-cost clay 3D printers [28].

We first developed a *bronze metal clay*—created from metal powder, binding agents, and water—that can be printed using desktop clay 3D printers. This hand-made metal clay is easy to make from readily available ingredients that are significantly less expensive than other printing materials. Table 1 shows a summary of the cost of different materials, including the "Bronze Filamet" offered by Virtual Foundry [34] and Bronze powder, the primary ingredient in our recipes[2]. As can be seen in the table, other materials are 4 to 5 times as expensive as bronze powder.

Other notable benefits of our CeraMetal approach include a workflow in which our bronze clay can be easily printed with desktop clay 3D printers that are significantly cheaper than printers used for SLS and BMD printing as showcased in Table 1. Moreover, our bronze clay can be quickly and easily recycled without the need for special tools or expertise, reducing material costs and promoting environmentally sustainable prototyping and production.

The primary contribution of this paper is the introduction of CeraMetal—a new robust and easy-to-implement system for desktop 3D printing in metal. To support this contribution, we introduce and compare three bronze clay recipes that are suitable for 3D printing. We then detail the 3D printing process, which utilizes a custom slicing software that generates continuous extrusion toolpaths that support the rheological characteristics of the bronze clay. We go on to characterize the material properties including shrinkage, density, strength, and flexibility of our 3D printed parts. Through these tests, we verify that CeraMetal produces metal parts with similar characteristics to other metal 3D printing processes. We then provide several example applications and lastly, discuss limitations and future research opportunities.

2 RELATED WORK

2.1 3D Printing, Materials, and Clay in HCI

Digital fabrication, including 3D printing, has long been a topic of interest within HCI [8, 59]. A subset of digital fabrication research in HCI has focused on the relationships between materials, machines, and software, leveraging material-based knowledge to expand and rethink digital fabrication tools and processes. Work in this vein

[1]https://www.shapeways.com/

[2]The cost of other ingredients in our recipes is negligible compared to metal powder.

has turned to materials science, craft tradition, and artistic practice for inspiration, cf. [2, 19, 23, 94].

Of particular relevance, a growing body of work is exploring the use of clay and clay-like materials in digital fabrication. A variety of approaches to clay 3D printing have been developed, but in the most popular method, a Direct Write (DW) printer extrudes a softened clay to build forms [15]. A number of commercial user-friendly clay 3D printers have been introduced in the past several years, including machines by 3D Potter[3], WASP[4], Eazao[5], Lutum[6], and TronXY[7].

HCI researchers employing clay 3D printers have developed special purpose Computer Aided Design (CAD) and Computer Aided Manufacturing (CAM) software, designed to exploit clay's unique material characteristics and facilitate the design of new kinds of clay artifacts [10]. Clay 3D printing has also served as a new way to explore data physicalization [21, 22], architectural design [25, 68], and creative expression [49, 69].

Researchers are also employing similar digital fabrication approaches to develop and explore novel clay-like materials. 3D printable biomaterial "clays" that are recyclable, repairable, and compostable have been developed [11, 73, 75]. Novel clays, pastes, and foams have also been developed outside of the 3D printing context [7, 51]. Our 3D printable metal clay and accompanying workflow contributes to work in these traditions, blending material design, digital fabrication, and software development.

2.2 Gcode Generation

When 3D printing with a novel material, it can be useful to create custom toolpaths (.gcode files) instead of using traditional slicing software [11, 41]. Custom toolpaths enable the creation of forms that cannot be produced with traditional slicers. For example, Bourgault et. al's CoilCam, a tool optimized for clay 3D printing, generates vessels with complex forms and surface textures by applying a series of mathematical operations to cylinders [10]. Other design tools that generate .gcode have been developed to create objects with a range of mechanical characteristics from traditional FFF printers. Takahashi and Miyashita explored emergent material properties created by a range of non-traditional toolpaths [79]. "Meta-materials" generated from PLA filament on FFF printers include textiles [32], foams [55], and hair-like structures [65]. As with CoilCam, these are special-purpose design tools rather than general-purpose slicers.

Novel general-purpose slicers have also been developed. For example, Vespidae is a suite of tools that enables working with multiple materials and fabrication machines on a single design [33]. One of its modules is a custom slicer and .gcode generator in which a user can choose the order in which different parts of a 3D model are printed. Xylinus is a plugin for Grasshopper that enables a designer to generate toolpaths (similar to those generated by a traditional slicer) directly from Grasshopper, eliminating the need for separate slicing software [44].

[3]https://3dpotter.com/
[4]https://www.3dwasp.com/en/
[5]https://www.eazao.com/
[6]https://vormvrij.nl/lutum/
[7]https://www.tronxy3d.com/products/tronxy-moore-2-pro-ceramic-clay-3d-printer

Our software, which we describe in more detail in Section 4.1, has a different aim and set of functionalities. It is a general-purpose slicer that produces toolpaths for solid, multi-walled, and hollow objects with *minimal travel movements*. Unlike the tools mentioned above, it is designed specifically to support the 3D printing of rheologically non-linear materials like CeraMetal. It is possible to use Vespidae to manually eliminate some travel paths in a 3D print by carefully specifying (by hand) the order in which geometry is printed. However, the slicing algorithm itself does not reduce travel paths. Xylinus can translate curves generated in Grasshopper or Rhino into .gcode. But, like Vespidae, its slicing algorithm does not reduce travel paths. It is worth noting that any slicer—including Vespidae, Xylinus, Cura, and Simplify 3D—can generate one kind of toolpath with few travel moves, using a "vase mode" or "spiralize outer contour" setting, where the toolpath spirals up along the outside of a form. However, this functionality only works for simple (non-branching) geometry and can only generate hollow toolpaths. The approach provides no way to generate complex forms or solid or infilled structures.

2.3 Metal 3D Printing

Rudimentary "3D printing" of metal predates modern digital fabrication technology. A 1925 Patent describes building 3-dimensional artifacts with layers of welding beads [70], and in 1976 Dimetto described stacking layers of precisely cut sheet metal to create forms [24]. The approaches that are most widely used today were developed in the 1990s and include Selective Laser Sintering (SLS), Selective Laser Melting (SLM), and Electron Beam Melting (EBM). In these powder-based approaches, a part is built up from layers of sintered or melted metal powder. Binder jetting is another powder-based approach in which a liquid adhesive binds metal powder into an initial shape. The binder is removed during a debinding step–the binder is either dissolved with a chemical solvent or burned away, and the metal is sintered in a furnace to produce a solid part [17, 37].

The category of material extrusion (ME) includes techniques in which forms are constructed from layers of material extruded through a nozzle [45, 50, 71]. In the Fused Filament Fabrication (FFF) approach to metal 3D printing—referred to as Bound Metal Deposition (BMD) [85]—a custom filament, consisting of metal powder blended with a wax/polymer binder, is rigid until it reaches a heated nozzle, at which point the binder melts and the binder/powder mixture is deposited. As in the binder jet process, the binder must be removed and parts must be sintered after printing. Printers, materials, debinding stations, and furnaces for BMD are offered by Desktop Metal [60, 61]. Companies like Virtual Foundry have developed metal filaments that can be used in standard FFF machines [34].

Direct Ink Write (DIW or DW) printing—also known as Robocasting [67]–is another ME technique in which parts are built from an extruded paste [72]. DW printing is a popular approach to food printing [52], bio-materials printing [75], and ceramics printing [15]. This approach has also been employed to 3D print liquid metals [64]. Only a handful of researchers have explored a DW approach similar to the one we describe here, primarily in the context of very specific applications [20, 54]. It remains an under-explored area. Our DW metal clay approach was inspired by the increasing

availability of low-cost consumer-grade clay 3D printers (cf. [28]) and the history of jeweler's metal clay.

2.4 Jeweler's Metal Clay

Jeweler's metal clay (JMC) is a malleable material that can be sculpted into 3D forms and then fired into a solid metal. Scientists working for Mitsubishi developed the first metal clay out of gold in 1994, terming it "precious metal clay" (PMC) [29, 42]. PMC is now available in gold and silver [77]. Since its introduction, a range of similar materials have been developed. The company Art Clay offers silver and copper clays, while Metal Adventures and Prometeus Clay offer bronze and copper-based varieties [77]. Goldie has developed a series of copper, bronze, and iron-based clays [16]. Hadar Jacobson sells powders that can be mixed with water to form clay in a range of metals [47]. JMC must go through a debinding and sintering process before becoming solid metal. These steps are typically achieved through a custom firing process in a kiln [30].

JMC is widely used by jewelers to create delicate sculptural forms and detailed surfaces [39, 46, 88]. The vibrant metal clay jewelry community has its own international guild, the Alliance for Metal Clay Arts Worldwide [31], and many dedicated websites provide platforms for knowledge sharing and discussion–cf. [1] and [13]. A variety of books are also available, covering techniques that include pressing textures into JMC [40], carving JMC with channels that are then filled with enamel [27], and forming JMC structures around gemstones [6].

JMC is unsuitable for 3D printing; it is much too hard, sold only in very small quantities, and very expensive—a standard 100g gram package of BRONZclay™, which contains approximately 10 cm^3 of bronze, sells for around $24 [77]. In contrast, 100g of bronze powder is approximately $4. We found one documented attempt to print a diluted metal clay in a student thesis project, but prints suffered from severe slumping and very low print quality [36]. Nevertheless, we have found the JMC community a valuable source of technical knowledge and creative inspiration.

3 DEVELOPING 3D PRINTABLE BRONZE CLAYS

To develop a bronze clay suitable for 3D printing with available desktop printers, we had to (1) identify ingredients, (2) formulate recipes that were optimized for both printability and sinterability, and (3) develop methods for mixing clay and ensuring the consistency of our recipes.

3.1 Ingredients

The primary ingredient in our bronze clay is *bronze metal powder* sourced from Metal Powders USA [83]. This powder is 325 mesh (particles are less than 45 μm in diameter), and consists of a mixture of tin (10-11%) and copper (89-90%)[8]. Metal powder must be mixed with a *binder* to become metal clay. Binders are critical ingredients that bind metal particles to each other when the mixture is combined with water, giving the material its clay-like consistency. Previous analysis identified the binder used in commercial BRONZclay™ as methylcellulose [36]. *Methylcellulose* is a thickener and emulsifier commonly used in food and cosmetic products that is derived from plant and vegetable cellulose [63]. *Xanthan gum* is another thickener and emulsifier often used in the food industry. It is a natural biopolymer that is created when sugar is fermented via a bacteria called Xanthomonas campestris [48]. Both materials have been used as binders in other custom materials designed for 3D printing [54, 73]. The final ingredient in our clay is *water*. Methylcellulose and xanthan gum dissolve in water, forming a gel that surrounds and binds granules of metal powder, thus creating a clay-like substance that is suitable for extrusion.

When designing a material for 3D printing, one must carefully control the rheology of the material. Rheology describes the way a material flows in response to applied force and determines how a material will flow through a printer. Methylcellulose and xanthan gum, when mixed with water, have slightly different rheological characteristics, but both materials exhibit complex non-linear behavior and can have shear thinning characteristics under the right circumstances [63, 92]. A shear thinning material behaves more like a liquid under stress and more like a solid when the stress is removed. This is an good characteristic for a 3D printing material as it makes the material relatively easy to extrude–the material behaves like a liquid as it is forced through a printer–and stable once printed–it behaves more like a solid when the extrusion forces are removed.

3.2 Health Concerns and Safety Precautions

Working with metal powders can present significant health risks. Of particular concern are the risk of the combustion of metal dust and health risks due to the inhalation of metal powder. The severity of the risk depends on the type of metal and the particle size. The smaller the particle size, the deeper the level of penetration into the lungs. Particles less than 10μm in diameter (of any material) can get into the pulmonary system if inhaled [81] and are considered particularly dangerous. Nano-particles—with a diameter less than 100nm—are considered even more dangerous, with potential health effects that are not yet well understood [9, 38].

Bronze powder is a relatively benign metal powder, but care must still be taken in its handling. Bronze powder poses no known risk of explosion; it is classified as non-flammable. It is also classified as non-hazardous. However, eye irritation and skin irritation can result from handling and respiratory irritation can result from the inhalation of powder [76, 82]. Our 325 mesh Bronze powder has a maximum particle size of 45μm (note that the mixture may include smaller particles) [83]. The material's Safety Datasheet specifies that one should "avoid breathing dust, use in a well ventilated area, wash hands thoroughly after handling, and wear protective glasses and gloves" [82]. We use eye protection, gloves, and respirators when working with bronze powder and strive to minimize the creation of dust.

Once the material is in clay form, the risk of inhalation is eliminated and the material is safer to handle. The SDS for BRONZclay™ does not include any protective equipment recommendations, but does advise people to wash hands after using [78]. We use gloves when handling the clay and take care to wash our hands after use.

[8]Trace quantities of other metals such as aluminum, manganese, nickel, or zinc may also be present.

	Methylcellulose	Xanthan Gum	Mixture
Bronze powder	100g / 70.0% volume	100g / 71.6% volume	100g / 71.0%
Methylcellulose	.5g / 4.6% volume	0	.17g / 1.5 %
Xanthan gum	0	.5g / 2.2% volume	.33g / 1.5 %
Water	9g / 25.6% volume	9g / 26.2% volume	9g / 26.0 %
Printing hardness (kg/cm^2)	.3	.4	.4
Hand feel	Clay-like, very sticky	Jello-like, smooth	Jello-like, slightly sticky

Table 2: Each of our three recipes has a slightly different binder.

3.3 Recipes

In developing a recipe for printable metal clay, we considered the following requirements based partly on an analysis by Duty et al. [26]:

(1) *Extrudability and Bead Functionality*: printer should extrude the material as a "bead" of consistent shape and size.
(2) *Structural Stability*: part should not collapse during printing.
(3) *Sinterability*: fired part should be solid metal. Sintering is a process through which metal powder coalesces into a solid metal when exposed to temperatures close to its melting point.
(4) *Dimensional Accuracy*: final part should have dimensions that correspond to the input model.

Through a series of preliminary experiments, we identified basic ratios of metal powder, binder, and water. This preliminary work was driven primarily by sinterability concerns. Binders can make up only a small percentage of the overall mixture in weight and volume. If too much binding material is added, metal will fail to successfully sinter during the firing process. We began by using a binder-to-metal powder ratio of 1 to 10, by weight, but these recipes did not successfully sinter. We gradually decreased the amount of binder to a ratio of 1 to 100. At this ratio, recipes with xanthan gum binders sintered, but the methylcellulose only recipe did not. We believe that this is due to the fact that methylcellulose is about half as dense (.40 g/cm^3) as xanthan gum (.84 g/cm^3)[9], which means it takes up twice as much volume per unit weight. Our final recipes are based on a binder ratio of .5 to 100 by weight–which corresponds to a maximum binder percentage by volume of approximately 5%. Our mixed recipe balances the amount of methylcellulose and xanthan gum by volume instead of weight, as this appeared to be the more important measure.

After we identified the basic .5 binder to 100 metal powder by weight–5% binder by volume–ratio we conducted more structured experiments with the three different recipes shown in Table 2. Each recipe uses a different binder though the overall ratio of binder to metal powder is kept fixed. The first recipe uses methylcellulose, the second xanthan gum, and the third a 1/3 methylcellulose to 2/3 xanthan gum blend. In Section 5, we characterize the material properties (e.g., shrinkage, density, and strength) of each recipe.

Figure 2: Recipe ingredients (top). Mixing ingredients in a kitchen mixer to form a uniform material with a clay-like consistency (bottom left). Measuring the indention hardness of the metal clay (bottom right).

When making clay, we typically use 500g of bronze powder and the corresponding amounts of other materials. We first combine the dry ingredients–metal powder and methylcellulose and/or xanthan gum, in a kitchen stand mixer. Then, we gradually add water while continuing to mix. Once a clay has formed, we continue mixing for at least one minute. We then measure the indention hardness of the clay to determine its suitability for printing [3, 18]. We used techniques described by Buechley and Ta to measure the hardness of our recipes using a penetrometer [11]. If necessary, we add water

[9]These measurements were taken in our lab. We also measured the density of bronze powder as 5.23 g/cm^3, and the density of water is 1 g/cm^3. All measurements were taken at room temperature.

to the mixture to achieve a printing hardness between .3 and .4 kg/cm^2. We found that we had to mix the methylcellulose-only mixture to a softer consistency than other materials to achieve extrudability. An overview of this process is shown in Figure 2.

We do not claim that these recipes are optimal. It is possible that the amount of binder in them could be decreased while maintaining printability. Reducing the percentage of binder used might improve some of the material characteristics we discuss in Section 5. We plan to continue to refine recipes in ongoing research. However, those shown in Table 2 produced reliable printable and sinterable materials and enabled us to conduct the printing experiments described in the rest of this paper.

3.4 Recycling and Reuse

Given the high cost of metal powder, it is cost-effective as well as environmentally sustainable to be able to recycle waste material instead of discarding it. Our clay-based approach enables us to easily recycle waste and unwanted parts, *as long as they are not yet fired.* Print waste is collected, ground in a blender or food processor, and remixed into clay, see Figure 3. Grinding waste product back into a powder is a process that can release bronze dust. During this process, a respirator and eye protection should be worn.

Figure 3: Process for recycling un-sintered bronze clay. Print waste is collected (left), ground back into powder using a blender (center), and then mixed with water to form a recycled clay (right).

We have found that bronze metal clay can undergo at least three recycling cycles before exhibiting any obvious signs of degradation and we have not experienced any sintering problems when employing recycled clay. However, bronze will eventually oxidize when exposed to water and air, so we believe that there is a limit to the number of recycling cycles that can be undertaken and hope to address this in future research. To minimize oxidation, we keep printed clay waste dry until it is ready to be remixed and reprinted. None of our technical tests were conducted with recycled clay, but some of our application examples were printed with reused material.

Sintered metal parts cannot be easily recycled back into clay. After sintering they are solid metal. These parts can be recycled like traditional metal wares or ground back into powder using specialized equipment.

4 3D PRINTING BRONZE CLAY

The characteristics of 3D printed objects depend not only on the materials they are made from, but also how they are printed. To successfully print parts from our bronze clay, we had to create custom CAM software and make small modifications to existing 3D printers.

4.1 Custom Slicer: Generating Continuous Extrusion Toolpaths

To 3D print an artifact, the user first employs CAD software to design the artifact's geometry. The resulting 3D model is then sent to CAM software, a slicer, which generates a toolpath for the 3D printer. The output of the slicer is a .gcode file that specifies: (a) the path the 3D printer will take and (b) material extrusion along that path.

Our metal clay and the Direct Write (DW) printer we are using have important properties that are not taken into account by traditional slicing software, which was designed for thermoplastics and FFF printers. One of the most important differences is that, while it is easy to start and stop the extrusion of thermoplastics, it is challenging to start and stop the extrusion of soft materials like clay. Extrusion behavior depends on the rheology of the material. Materials with non-linear rheological characteristics (such as our bronze clay) can be particularly challenging to work with. Significant delays between when a start or stop extrude action is executed by the printer and when the material reflects this action are common. For instance, the material often continues to ooze out of the nozzle long after a stop extrusion command is given.

Toolpaths generated by traditional slicers assume that extrusion can be stopped and restarted instantly. As a result, the paths they generate contain many travel moves, where the print head must move from one location to another without extruding. Because DW machines cannot reliably stop extruding, toolpaths with travel moves typically result in print failures. Traditional slicing software does not currently provide control over travel moves or provide the capability to generate continuous extrusion paths. To address these challenges, we developed a custom slicer that generates *continuous extrusion toolpaths*, thereby *minimizing travel moves*.

Our software is an open-source Python library designed to be used in conjunction with Grasshopper and Rhino. Our software works in many ways like a traditional slicer. See Figure 4. A user of the library imports a 3D model and sets values for the parameters, shown in Figure 4. A *shrinkage* parameter sets the shinkage rate and is used to resize the model to take account of shrinkage that happens during firing. The *solid/hollow mode* parameter specifies whether the generated part is solid. The user can also specify the *number of walls* their print should have in hollow mode. The user can also set a number of standard print parameters including the *printer* being used, the *nozzle size*, *layer height*, *speed*, etc.

Our software uses these values to first slice the part into horizontal layers. The toolpath that is generated for for each layer has no travel moves. We use an approach described by Zhao et al. [91] to generate these paths. Our algorithm first creates the contour curves for a layer. Then, it constructs a continuous spiraling path based on these contour paths, using Fermat spirals. A Fermat spiral is a space-filling curve that consists of two matched spiral paths, one that goes inward and one that goes outward [53], as demonstrated in Figure 5. The output of the software is a .gcode file that can be

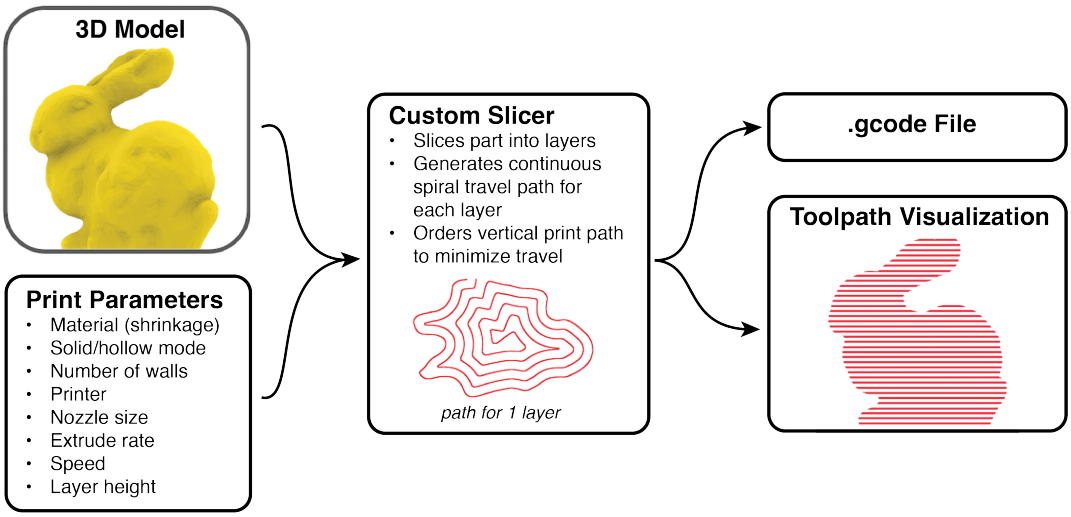

Figure 4: Our software workflow

sent to a 3D printer and a 3D visualization of the print path that can be viewed in Rhino.

Our software includes printer profiles for several different machines, including the Eazao Zero, the printer we use in the experiments presented here. Our software can be used to create continuous travel toolpaths for most 3D printers and a range of materials. Our software does not include support generation capabilities, so our ability to generate toolpaths for shapes with significant overhangs is limited.

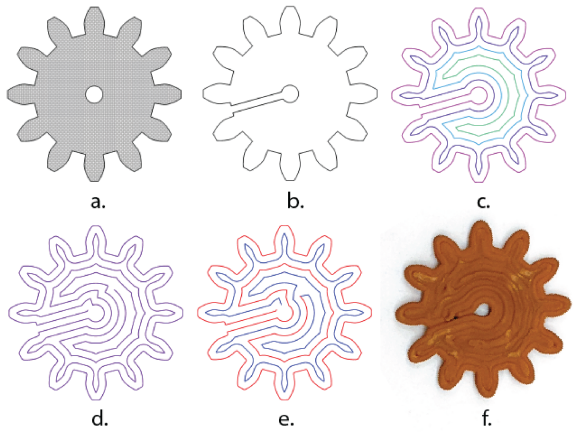

Figure 5: A diagram showing the steps taken by our slicing algorithm for one layer. (a) The part. (b) Holes in the layer are connected to create a single continuous closed path. (c) Contour curves are generated. (d) Contour curves are connected to create a spiral. (e) A fermat spiral is generated. The inward spiral is shown in red and the outward spiral is shown in blue. This is the complete path for the layer. (f) A top view of the 3D printed part.

4.2 Printing and Drying

Once a toolpath is generated, it is sent to a 3D printer. We used an Eazao Zero clay 3D printer for the experiments described in this paper. We chose the Eazao Zero because it is a small, low-cost, clay 3D printer that is readily available. However, any direct write clay 3D printer with auger-based extrusion could be substituted in our workflow. This includes printers by TronXY, WASP and Lutum. For clay 3D printers without augers, like most Potter Bot models, extra care would need to be taken to remove all air bubbles from the metal clay before printing.

The process of printing our bronze clay is similar to that of printing traditional clay. The bronze clay is loaded into the print tube, and then a plunger forces the material from the print tube, through the connector tubing and into the extruder, where the auger pushes the material out the printer nozzle. A print parameter called mix-factor, which is set in the .g-code file, determines the relative speeds of the stepper motors driving the plunger and auger to extrude the material.

To achieve more stable prints, we built a custom heater and attached it to the print head with magnets, see Figure 6. The heater consists of two fans that blow air across coils of nichrome wire. The heater improves the structural stability of prints by partially drying each layer of a part as it is constructed.

Unless otherwise noted, we printed our metal clay with a 0.61mm inner diameter nozzle (a 20 gauge syringe tip). We also used the following settings: a mix-factor of 0.96 (auger) to 0.04 (plunger), an extrude rate of 0.25 mm of filament extruded per 1 mm traveled, a speed of 800 mm/minute, and a layer height of 0.45 mm. We printed parts on a thin cotton fabric, which enabled us to easily remove parts from the build plate and expose all part surfaces—including the bottom—to air during the drying process.

Once a part has finished printing, it must be completely dried before it is fired. To ensure quick and reliable drying, we place parts on a rack in a small food dehydrator set to 110°F (38°C) until they are dry. After a part has been printed and dried, it is in its "green" state. It is a reasonably stable solid, but not yet metal. In the green

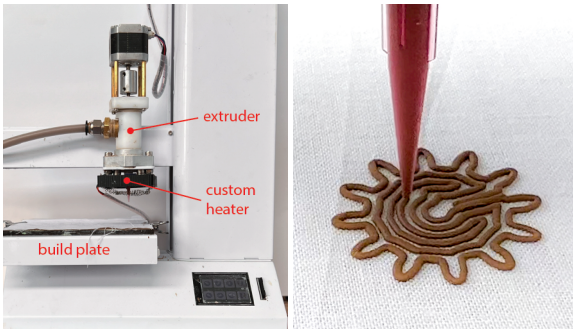

Figure 6: Left: our printer. Right: a close-up showing material being deposited by the nozzle. This image also highlights the spiral nature of our slicing algorithm, showing the inward spiral for the first layer of a gear print.

state, parts can be broken and should be handled with care before firing.

4.3 Debinding and Sintering

As with JMC, our bronze clay needs to be fired to transition from bound metal powder to solid metal. During firing, first debinding occurs when the binding ingredients (methylcellulose and xanthan gum) are burned away. Then, the metal powder is sintered. Sintering is a process in which particles join together to form a solid without melting. Sintering occurs when a metal powder reaches a temperature close to, but just below, its melting point. Energized particles begin to bond to one another, coalescing into a solid before reaching the material's melting phase [35].

Figure 7: Parts are buried in activated carbon before firing.

Our material blends are similar enough to JMC that we were able to leverage knowledge from this community to develop reliable debinding and sintering processes. Our firing was done in a small potter's kiln, a Skutt KM–614–3[10]. Debinding and sintering both take place during a single "ramp-hold" firing process known as a firing schedule. We ramp at 250°F (121°C) per hour to 1000°F (538°C) and hold this temperature for two hours–this constitutes the debinding step. We then ramp at 200°F (93°C) per hour from 1000°F to 1550°F (843°C)—the melting temperature of bronze is 1675°F (913°C)—and hold this temperature for four hours. This constitutes the sintering step. The material is then left to cool back to room temperature before it is removed from the kiln. The entire firing and cooling process takes approximately 20 hours.

If parts are fired in open air inside the kiln, the metal powder will oxidize before it sinters. Firing must take place in an environment free of oxygen to avoid oxidation. We address the oxidation challenge by burying "green" (unsintered) parts in a bed of activated carbon, inside a stainless steel container, as shown in Figure 7. We note that the container must be made from a material that has a significantly higher melting point than the metal part to be sintered; such as stainless steel, which has a melting point of approximately 2550°F (1400°C), significantly higher than bronze. During firing, the activated carbon consumes oxygen in the kiln, preventing the formation of oxides [30]. The type of carbon used, the size of the part, the amount of carbon surrounding the part, and the firing hold-times can all impact sintering quality. For bronze clay, we use activated carbon derived from coconut shells and surround each part with at least 15 mm (.5 inches) of carbon on all sides.

There are future research opportunities in fine-tuning this firing schedule to optimize final material properties. We can likely obtain harder, denser, and more elastic bronze by changing the firing schedule. Previous research on the sintering of metal powder has demonstrated that small changes in the firing schedule can significantly impact material properties [35, 50, 86].

4.4 Optional Post Processing

Once parts have cooled and are removed from the kiln, like any metal that has been worked with heat (i.e., through casting or soldering), they will have a colorful surface patina. Sintered parts can be cleaned and polished using traditional metal working approaches. A standard approach to cleaning is to soak parts in a "jewelers' pickle"—a mild acidic bath–to remove patina and "fire scale" [43, 57]. Figure 8 shows parts after printing (top) and after firing with the patina (middle) and without (bottom).

If desired, sintered parts can also be polished and modified using traditional metal-working techniques. For example, they can be polished with metal brushes, steel wool, or files. Work can be done either by hand or using equipment like jewelry polishers. All post processing is optional and for cosmetic purposes. Parts are fully functional once they are sintered.

Figure 8: Three wrenches, from top to bottom: after printing, after firing, and after cleaning

[10]https://skutt.com/products-page/ceramic-kilns/km-614/

5 MATERIAL CHARACTERIZATION

For each of our 3D printable bronze clay recipes, we ran tests to characterize and compare their printing behavior and mechanical properties including shrinkage, density, strength, and flexibility. Most of these tests are standard mechanical tests that are conducted to understand and compare material properties. Our primary aim was to verify that parts made with our material and workflow are comparable in quality to other 3D printed and sintered metal parts. We wanted to verify that our materials and workflow produce useable parts with reasonable mechanical properties.

5.1 Printing Behavior

Each of the three different materials has a slightly different printing behavior. The methylcellulose only recipe seemed to require more force to extrude than other materials. We were unable to develop a successful method for measuring force or system pressure directly. However, we found that the methylcellulose-only recipe needed to be mixed to lower hardness value than other recipes to successfully extrude. This experience aligns with previous research. Xanthan gum is known to increase a mixture's shear thinning behavior, both alone and when mixed with methylcellulose [92]. The presence of xanthan gum in a recipe seems to help metal clay flow more readily through the printer. The methylcellulose-only recipe was the most challenging material to print and the xanthan-gum-only recipe was the easiest material to print. However, we were able to consistently print all recipes.

5.2 Shrinkage

Careful characterization of a material's shrinkage behavior is essential for designing and printing dimensionally accurate parts. A design is resized according to shrinkage rates before printing so that after the material has been sintered it will have exactly the intended dimensions. We measured the shrinkage behavior for three different forms: solid cubes (10mm x 10mm x 10mm), hollow cylinders (20mm x 20mm x 20mm), and solid dog bones (130mm x 12.5mm x 2mm). We printed five samples of each shape for each material. Figure 9 shows images of each of the parts, with the measured dimensions indicated. We calculated the linear shrinkage for X, Y, and Z using equation 1:

$$\text{linear shrinkage} = \frac{\text{dimension of green part - dimension of fired part}}{\text{dimension of green part}} \quad (1)$$

Figure 10 shows the amount of shrinkage that we observed for each of our parts and materials. Planar (XY) shrinkage is shown in orange and vertical (Z) shrinkage is shown in yellow. We averaged the X and Y shrinkage measurements for the cubes and cylinders because these measurements were indistinguishable from one another. For the dog bones, we measured shrinkage only along the length (X) direction.

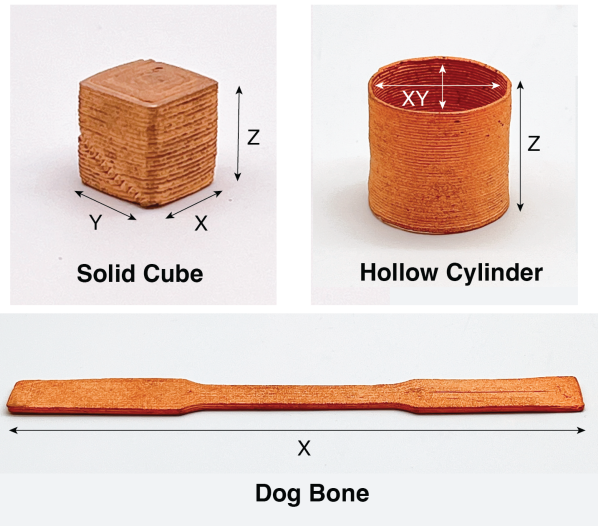

Figure 9: The parts we used to calculate shrinkage. Measured dimensions are labeled. We measured only the shrinkage in length (X) for the Dog Bones.

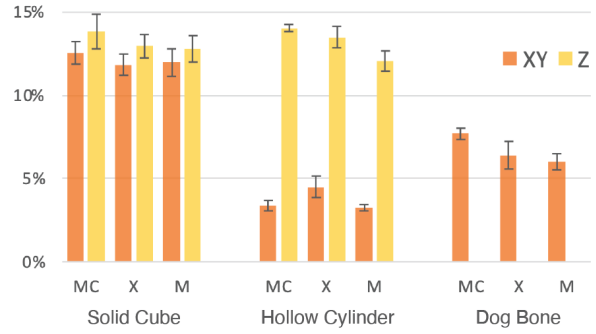

Figure 10: Shrinkage for three different parts printed in our three materials. MC = Methylcellulose, X = Xanthan Gum, M = Mixture. Planar (XY) shrinkage is shown in orange and vertical (Z) shrinkage is shown in yellow. N=5 for each condition.

The shrinkage rate for all materials is anisotropic and varies with part geometry. We observe fairly consistent vertical shrinkage rates for all geometries and vertical shrinkage is always higher than planar shrinkage. We observe the largest planar shrinkage rates for the solid cubes. We observe significantly less planar shrinkage for the dog bones and cylinders. We believe that the cylinders may be particularly restricted from shrinking in the planar dimension because their centers are filled with carbon during sintering, which likely restricts planar movement.

For each geometry, the shrinkage rate between recipes is similar–often within the observed margin of error. The fact that we obtain different shrinkage orderings for different parts (i.e., higher planar shrinkage rates for methylcellulose for cubes but not for cylinders) leads us to believe that the differences between materials is likely within the margin of error for our testing procedures.

Our observations are consistent with previous research, which has shown that sintered metal parts (including 3D printed and sintered bronze) experience anisotropic shrinkage and that the

largest shrinkage occurs in the z dimension [74, 86, 90, 93, 93]. This is due to the fact that gravity compresses the parts vertically during sintering. Generating dimensionally accurate parts with arbitrary geometries from 3D printed and sintered metal typically requires the development of a complex resizing model that takes anisotripic shrinkage into account (cf. [90]).

5.3 Density

A traditional measure of the quality of metal 3D prints is relative density, a comparison of the density of metal prints to that of solid bronze. Higher density indicates a better sintering result. Lack of relative density indicates undesirable porosity, which can occur due to imperfect print parameters–small air pockets can be trapped between vertical or horizontal layers of a part [86]. Porosity can also arise from material dynamics–air pockets can form within the print material during the debinding and sintering process as the binder burns away and metal particles fuse together [58].

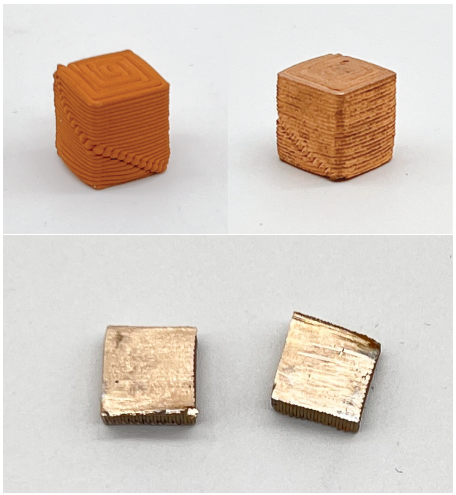

Figure 11: A 10mm cube after printing (top left) and after sintering (top right). A cube cut in half (bottom).

We measured the density of our cubes using Archimedes' principle, a standard method of determining the density of sintered and cast metal parts [5]. Samples were weighed first in air and then submerged in water. We used a value of 0.998 g/cc for the density of water, which is its rated density at 68°F (20°C) [12], and then calculated density using Equation 2:

$$\text{Density of part } (\rho) = \frac{\text{mass in air * density of water}}{\text{mass in air - mass in water}} \quad (2)$$

The density of bronze varies as a function of the percentage of Tin (Sn) to Copper (Cu) in the alloy. A Bronze with 14% Sn and 86% Cu has a density of 7.4 g/cc, and with 8% Sn, a density of 8.9 g/cc [80]–Copper is denser than Tin. Our bronze metal powder contains between 9 and 11% Sn [82]. We assume a 10% Sn content and use an ideal density of 8.4 g/cc as our theoretical solid bronze density to compare against. Relative density is calculated with respect to this value.

Table 3 shows the results of these tests. The material with a methylcellulose-only binder has the highest density, followed by the xanthan gum material and then the mixture, but the measurements for all three materials are very similar and within the margin of error for our tests.

Material	Measured density (g/cc)	Relative density (%)
Methylcellulose	7.66 ± .18	91.2% ± 2.0%
Xanthan Gum	7.62 ± .09	90.7% ± 1.1%
Mixture	7.52 ± .35	89.5% ± 4.2%

Table 3: Measured and relative densities for each of our materials. Relative density = Measured density / solid bronze density. N=5

These results are positive and align with previous research. Our materials exhibit similar and, in many cases, higher density compared to other 3D printed and sintered bronzes. Wei et. al. recorded the density of parts printed with Bronze Filamet™ on FFF machines as between 6.5 and 6.9 g/cc [86]. The density of sintered bronze made through traditional powdered metallurgy approaches–through sintering compressed bronze powder as opposed to 3D printing–is typically between 5.5 and 6.75 g/cc [4]. Kilinc et al. printed a custom bronze filament–made from a mixture of bronze powder and a wax polypropelene binder–and obtained a density of 7.1 g/cc using a sintering temperature of 850°C (1562°F), very similar to ours. Notably, they were able to increase the density of their parts to 8.27 g/cc by increasing their sintering temperature to 900°C (1650°F). However, parts experienced more distortion at higher temperatures. We may be able to increase the density of our parts by increasing our sintering temperature.

5.4 Strength and Flexibility

Metal is a useful material in large part because of its strength and flexibility. To determine if our 3D printed parts were as strong as traditional bronze, we ran uniaxial strength tests based on the standard, ASTM E8 [11], for tensile strength testing of metallic materials. To do so, we printed the dogbone shape dictated by the standard in each material, as shown in Figure 12. We then loaded each specimen into a universal testing machine fitted with a 50 kilonewton force load cell, which pulled the specimen apart at a rate of 0.01 mm/sec. We recorded the tension force applied until failure (i.e., breakage). From this, we obtained the maximum force applied to the cross-sectional area of the specimen, which we used in Equation 3 to calculate maximum tensile strength.

$$\text{max tensile strength (MPa)} = \frac{\text{max force (N)}}{\text{cross-sectional area (mm}^2\text{)}} \quad (3)$$

[11] https://www.astm.org/e0008_e0008m-22.html

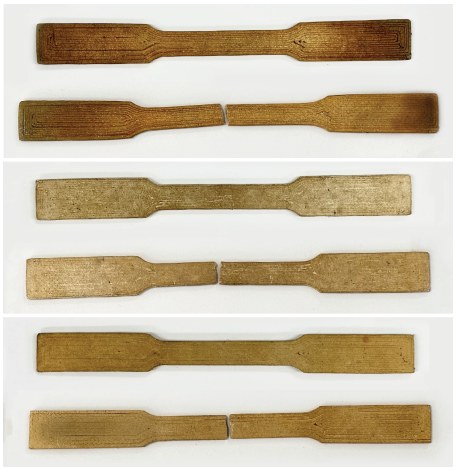

Figure 12: Test specimen for each recipe before and after testing: Methylcellulose (top), Xanthan Gum (middle), Mixture (bottom).

We also looked at the flexibility of our specimen, which is measured by the percent elongation at break. This elongation can be seen in Figure 12, where a specimen of each recipe is shown before and after testing. We calculated flexibility using Equation 4:

$$\text{flexibility (\%)} = \frac{\text{initial length} - \text{length at break}}{\text{initial length}} * 100 \quad (4)$$

We tested three specimens for each material, the average strength and flexibility are presented in Table 4. Previous research has reported a range of values for the tensile strength of 3D printed and sintered bronze, with strength values changing significantly with sintering temperature. Our measurements are within these ranges. At sintering temperatures close to our temperature of 843 °C, Kilinc reports a tensile strength of 77 MPa at 850 °C [50] and Lostado 79 MPa at 841°C and 105 MPa at 858 °C [56]. Tensile strength increases with sintering temperature—Wei achieved approximately 150 MPa at 871 °C [86] and Kilinc achieved 212 MPa at 900 °C. Elongation also increases with sintering temperature. Kilinc reports an elongation at break value of 11.4% at 850 °C and 35.7% at 900 °C. We expect that we could increase the strength and elasticity of our materials by increasing our sintering temperature.

Material	Maximum Tensile Strength (MPa)	Flexibility (% Elongation)
Methylcellulose	119.66 ± 7.52	9.20 ± 0.80
Xanthan Gum	99.09 ± 8.83	2.93 ± 0.46
Mixture	117.40 ± 5.54	4.40 ± 0.69

Table 4: Tensile strength and elongation at break for each of our materials. N=3

It is notable that the material with a methylcellulose-only binder was significantly stronger and more flexible than the others and the xanthan gum based material was the weakest and least flexible.

5.5 Recipe Comparison

The most important outcome of our tests is that all of our recipes produce viable bronze parts. The shrinkage, density and tensile strength of our parts are similar to those of other 3D printed and sintered bronzes. There is little difference between the three recipes for most of the variables we studied. The xanthan gum based recipe is slightly easier to 3D print, but this material also seems to be weaker and less flexible than other recipes. For the applications we present in this paper, and likely most of the applications of interest to HCI researchers, there is no overwhelming reason to choose one of our recipes over another. If ease of printing is prioritized, a recipe with xanthan gum may be slightly preferable, but if high flexibility is important, the methylcellulose may be best.

Further research should be conducted to more comprehensively characterize shrinkage behavior, determine an optimal firing schedule, and identify trade offs between sintering temperature, density, strength, and dimensional accuracy.

6 APPLICATIONS

We printed a range of objects to test the viability and range of our material and workflow. All applications were printed with the metal clay material that utilizes a mixture of methylcellulose and xanthan gum as the binder.

6.1 Functional Metal Parts: Tools and Gears

One of the appeals of metal 3D printing is the ability to print functioning metal parts like mechanical components and special-purpose tools. To test our approach for these contexts we printed a wrench and a set of functioning metal gears.

Figure 13: Top: using a 3D printed wrench on a Dremel tool. Bottom: two gears driven by a stepper motor.

We recently lost the wrench that fits the Dremel tool in our lab–size 3/8 SAE, 10mm metric–a critical component required to swap out attachments. Rather than order a replacement, we printed one. We downloaded a wrench design (as a .dxf file) from McMaster Carr[12] and resized it. We resized the model using a 6.0% shrinkage rate, the observed shrinkage in length for our dog bones printed from the same material—the wrench is a similar size and thickness. The printed wrench functioned as intended immediately after printing, requiring no sizing adjustments. We have since been using it regularly, see Figure 13.

We also printed a set of functional gears that were designed to be attached to a servo motor, see Figures 13 and 8. We employed web-based software to design the gears [84] and then imported the generated 2D drawings into Rhino. We used our software to create a 3D toolpath from the outlines. The main part of the spur gears and the rack are 3mm (6 layers) high. We added an additional 5 layers of support around the shaft hole. The spur gears–which measure 40mm and 57mm in diameter and have 12 and 18 teeth respectively–are designed to fit around either a 6mm (.25 inch) metal rod or the attachment on a medium-sized servo motor. We designed for these dimensions. Again, we resized each gear anticipating a shrinkage in XY of 6%. The final parts required a small amount of filing to fit onto the intended components.

Figure 14: A close-up view of one of our earring prints (top left), an assortment of earring prints (top right). Lab members modeling earrings and rings (bottom).

6.2 Precious and Delicate Artifacts: Jewelry

Metal, known for its durability and versatility, has long been regarded as a precious material. Its significance extends beyond its monetary value, particularly evident in the realm of jewelry where the preciousness of the materials goes beyond their economic worth.

As a nod to bronze's rich history as a precious metal, we designed a set of rings and earrings based on the polar rose equation $r = acos(n\theta)$ where $n = p/q$ and p and q are rational numbers [87]. a determines the maximum radius of the curve. For these very delicate prints, we reduced the extrude rate to .2 mm extruded to mm traveled and slowed the print speed to 400 mm/s. Each piece is 3-4 layers (2mm) tall. The plots are one extrusion (1mm) wide. For the earrings, a = 10mm and for the rings, a = 6mm. Figure 14 shows an assortment of these prints. All of them are left unpolished, thus embracing the surface patinas that make each piece of jewelry unique.

These fragile prints were challenging to handle until fired. We swapped our mesh fabric print bed for wax paper so that we could easily remove the prints from the bed for sintering. The earrings are lightweight and comfortable to wear.

6.3 Larger and More Complex Geometries

To explore the feasibility of printing and sintering larger parts, we designed a metal travel mug with an algorithmically generated surface texture. The texture is generated using a diffusion-limited aggregation cellular automaton. We use a model in which particles fall down from the top edge of a square and stick to particles that are already in place. Running the model results in a matrix indicating where aggregated particles are present. Our software generates an oscillating path at the diameter of the cup for each layer where the amplitude of the oscillation is increased by 1mm if a particle is present in the matrix.

The cup shown in Figure 15 is 90mm (3.5 inches) in diameter and 115mm (4 inches) tall. This print was printed using a 0.84mm inner diameter nozzle, an extrude rate of 0.4mm extruded per mm traveled, a layer height of 0.75mm, and a speed of 900mm/s. Using a larger nozzle made it easier to print a water-tight vessel because the

Figure 15: A cup with an algorithmically generated surface texture.

[12]https://www.mcmaster.com/products/wrenches/

extrusions for each layer were wider and more robust than those made with a 0.61mm nozzle.

Figure 16 shows a print of the Stanford Bunny model that is 60mm tall—the Stanford bunny being a notoriously difficult model to print successfully due to its overhangs. The toolpath for this print was generated with our custom slicing software in hollow mode with walls that are five layers thick. Figure 16 left shows the model during printing—note the visible wall thickness. We used a layer height of .3mm to achieve a higher resolution on this print and a mix factor of .97 auger to .03 plunger to compensate for the more tightly packed layers. The print experienced some slumping in the chest—where the overhang angle is steepest—but we were pleased with the overall print quality. It is similar in quality and model detail to prints produced by an FFF printer out of PLA.

Figure 16: A Stanford bunny during printing (left) and after sintering and cleaning (right).

7 DISCUSSION

7.1 Limitations and Considerations

While our approach is significantly cheaper than other metal 3D printing options, it is still expensive compared to plastic or ceramic printing. Our approach requires a kiln for debinding and sintering. Inexpensive clay printers currently cost at least $700 [13] and small kilns approximately $1000 [14], expenses that, while significantly less than a metal 3D printer, are nontrivial. However, both the clay 3D printer and the kiln can be used with clay and other materials. They need not be metal-specific tools.

Metal is significantly more expensive than plastic or clay, even in powder form, and, as we described earlier, working with metal powder poses some safety risks.

Our metal prints are lower in resolution than those produced by more expensive printers. Resolution is limited by nozzle size on clay 3D printers. Though previous research found that one should be able to use a nozzle only two to three times a material's maximum particle size [14], we experienced nozzle clogging with nozzles smaller than .6mm in diameter. We have found that decreasing the layer height allows us to increase print resolution and that we can achieve a print quality close to that of traditional FFF printers using .4mm nozzles.

Our material is also limited in the types of geometries that can be printed. Because the clay remains soft during the printing process, it is challenging to create complex geometries with significant areas of overhang and our software does not currently include a support generation feature. Support structures could be manually added to 3D models, but these would still need to be printed from metal clay. Supports can be challenging to remove, which further complicates the creation of objects with overhangs, holes, or similar complexities.

Another limitation is that it is likely to be challenging to print large solid parts from metal clay. Because we are depositing a wet material that only dries fully after printing is complete, prints are subject to shrinkage before they are sintered. Solid parts thicker than approximately 1-2 inches (25-50mm) cannot be dried without significant cracking as the outside of a thick print dries before the inside and shrinks around it.

7.2 Future Opportunities

Our material tests illuminated several opportunities for future work. Additional technical tests could be conducted to: 1) fully characterize anisotropic shrinkage and develop a model for accurate three dimensional resizing, 2) investigate how the density, strength, and flexibility of our materials would change as a function of sintering temperature, and 3) better understand how the binding ingredients, methylcellulose and xanthan gum, impact material characteristics.

Our applications also bring attention to a variety of directions for expansion. For example, the gears demonstrated in Figure 13 are functional and sturdy. We built them as a proof of concept, but envision creating similar parts for real-world applications in the future. Similarly, we see ourselves continuing to use CeraMetal in the context of craft practices like jewelry making and further developing design workflows.

Though this paper focuses on a bronze metal clay, we can take a similar approach to develop 3D printable "clays" from other metals. Accordingly, we have begun to develop and test metal clays made from copper, brass, iron, and stainless steel. Because each metal clay mixture has a different rheological character, they need to be fine-tuned for printing. While we have begun to developed recipes for some of these other materials and are in the process of optimizing them for print quality.

One of the unique affordances of CeraMetal is that any paste-like material can be extruded by the printer. This means that we can design custom materials with similar rheological characteristics and combine them in a single print. We have begun to experiment with prints constructed from a blend of clay and bronze using a low-fire clay body that vitrifies (transforms from clay to ceramic) at a temperature similar to the sintering temperature for bronze. Figure 17 shows an image of a preliminary experiment. This fully sintered/fired cylinder (20mm in diameter by 100 cm tall) has a bottom 3/4 (orange color) of bronze and a top 1/4 (dark brown) of clay. We were surprised that this print did not break at the transition between the two materials during firing and are excited to continue exploring material blends.

[13] https://www.tronxy3d.com/products/tronxy-moore-2-pro-ceramic-clay-3d-printer
[14] https://skutt.com/products-page/ceramic-kilns/firebox-8x6-lt/

Figure 17: A sintered/fired print that combines bronze (bottom 3/4) and clay (top 1/4) in a single print.

We believe that the low-cost, accessible nature of CeraMetal will open up 3D printing with metal to new audiences in HCI and beyond. We specifically see metal 3D printing having an impact on the manufacturing industry when it comes to functional metal parts, especially parts that are difficult to manufacture through traditional methods such as machine milling.

We also envision metalworkers and jewelry makers adopting CeraMetal in their craft practices, just as clay 3D printing has been readily adopted by ceramic artists [10, 21]. It could potentially open up new commercial opportunities in (computational) design and support a range of new design workflows. We are excited to investigate these kinds of opportunities going forward.

8 CONCLUSION

In this paper, we present CeraMetal, a low-cost method for desktop metal 3D printing that employs a custom metal clay. We introduced three recipes for a printable bronze clay and demonstrated the versatility and robustness of our approach by printing several different designs. Our material analysis indicates that our parts have characteristics similar to those produced via other printing methods. We believe that this approach to metal printing provides new and valuable affordances to HCI researchers exploring digital fabrication including the ability to create custom material blends and to quickly and cheaply create metal prints using off-the-shelf printers and simple low-cost materials.

ACKNOWLEDGMENTS

This work is supported by National Science Foundation (NSF) Grant No. 2026218. We would like to thank Camila Friedman-Gerlicz, Alyshia Bustos, Erin McClure, and Alyssa Johnson - team members of the Hand and Machine lab.

REFERENCES

[1] Metal Clay Academy. 2018. Home | Metal Clay Academy. https://www.metalclayacademy.com/

[2] Lea Albaugh, James McCann, Lining Yao, and Scott E. Hudson. 2021. Enabling Personal Computational Handweaving with a Low-Cost Jacquard Loom. In *Proceedings of the 2021 CHI Conference on Human Factors in Computing Systems (CHI '21)*. Association for Computing Machinery, New York, NY, USA, 1–10. https://doi.org/10.1145/3411764.3445750

[3] F. A. Andrade, H. A. Al-Qureshi, and D. Hotza. 2011. Measuring the plasticity of clays: A review. *Applied Clay Science* 51, 1 (Jan. 2011), 1–7. https://doi.org/10.1016/j.clay.2010.10.028

[4] Copper Development Association. 2023. Industrial Powder Metallurgy - Characteristics and Properties of Copper and Copper Alloys. https://www.copper.org/resources/properties/129_6/characteristics_properties.html

[5] ASTM. [n. d.]. ASTM B962: Standard Test Methods for Density of Compacted or Sintered Powder Metallurgy (PM) Products Using Archimedes' Principle. https://www.astm.org/b0962-17.html

[6] Lisa Barth. 2011. *Designing From The Stone: Design Techniques for Bezel Setting in Metal Clay Using the Stone as Inspiration.* CreateSpace Independent Publishing Platform.

[7] Fiona Bell, Netta Ofer, and Mirela Alistar. 2022. ReClaym our Compost: Biodegradable Clay for Intimate Making. In *Proceedings of the 2022 CHI Conference on Human Factors in Computing Systems (CHI '22)*. Association for Computing Machinery, New York, NY, USA, 1–15. https://doi.org/10.1145/3491102.3517711

[8] Bedrich Benes, David J. Kasik, Wilmot Li, and Hao Zhang. 2017. Computational Design and Fabrication. *IEEE Computer Graphics and Applications* 37, 3 (May 2017), 32–33. https://doi.org/10.1109/MCG.2017.50 Conference Name: IEEE Computer Graphics and Applications.

[9] J. Benson. 2012. Safety considerations when handling metal powders. *Journal of The South African Institute of Mining and Metallurgy* (2012). https://www.semanticscholar.org/paper/Safety-considerations-when-handling-metal-powders-Benson/905a9cfa594719ffe1a590bf5951824a1a4dce24

[10] Samuelle Bourgault, Pilar Wiley, Avi Farber, and Jennifer Jacobs. 2023. CoilCAM: Enabling Parametric Design for Clay 3D Printing Through an Action-Oriented Toolpath Programming System. In *Proceedings of the 2023 CHI Conference on Human Factors in Computing Systems (CHI '23)*. Association for Computing Machinery, New York, NY, USA, 1–16. https://doi.org/10.1145/3544548.3580745

[11] Leah Buechley and Ruby Ta. 2023. 3D Printable Play-Dough: New Biodegradable Materials and Creative Possibilities for Digital Fabrication. In *Proceedings of the 2023 CHI Conference on Human Factors in Computing Systems (CHI '23)*. Association for Computing Machinery, New York, NY, USA, 1–15. https://doi.org/10.1145/3544548.3580813

[12] Canadian Conservation Institute (CCI). 2017. How to Determine Metal Density – Canadian Conservation Institute (CCI) Notes 9/10. https://www.canada.ca/en/conservation-institute/services/conservation-preservation-publications/canadian-conservation-institute-notes/metal-density.html Last Modified: 2017-09-11.

[13] and Jewelry Central School of Art, Clay. [n. d.]. Metal clay classes and courses at CSACJ in Rushden. https://www.csacj.co.uk/

[14] Shareen S.L. Chan, Ryan M. Pennings, Lewis Edwards, and George V. Franks. 2020. 3D printing of clay for decorative architectural applications: Effect of solids volume fraction on rheology and printability. *Additive Manufacturing* 35 (Oct. 2020), 101335. https://doi.org/10.1016/j.addma.2020.101335

[15] Zhangwei Chen, Ziyong Li, Junjie Li, Chengbo Liu, Changshi Lao, Yuelong Fu, Changyong Liu, Yang Li, Pei Wang, and Yi He. 2019. 3D printing of ceramics: A review. *Journal of the European Ceramic Society* 39, 4 (April 2019), 661–687. https://doi.org/10.1016/j.jeurceramsoc.2018.11.013

[16] Goldie Clay. 2023. Goldie Iron. https://goldieclay.com/

[17] Suman Das, David L. Bourell, and S. S. Babu. 2016. Metallic materials for 3D printing. *MRS Bulletin* 41, 10 (Oct. 2016), 729–741. https://doi.org/10.1557/mrs.2016.217 Publisher: Cambridge University Press.

[18] Cláudio de Oliveira Modesto and Adriano Michael Bernardin. 2008. Determination of clay plasticity: Indentation method versus Pfefferkorn method. *Applied Clay Science* 40, 1 (June 2008), 15–19. https://doi.org/10.1016/j.clay.2007.06.007

[19] Ashley Del Valle, Mert Toka, Alejandro Aponte, and Jennifer Jacobs. 2023. PunchPrint: Creating Composite Fiber-Filament Craft Artifacts by Integrating Punch Needle Embroidery and 3D Printing. In *Proceedings of the 2023 CHI Conference on Human Factors in Computing Systems (CHI '23)*. Association for Computing Machinery, New York, NY, USA, 1–15. https://doi.org/10.1145/3544548.3581298

[20] Anagh Deshpande and Keng Hsu. 2018. Acoustoplastic metal direct-write: Towards solid aluminum 3D printing in ambient conditions. *Additive Manufacturing* 19 (Jan. 2018), 73–80. https://doi.org/10.1016/j.addma.2017.11.006

[21] Audrey Desjardins and Timea Tihanyi. 2019. ListeningCups: A Case of Data Tactility and Data Stories. In *Proceedings of the 2019 on Designing Interactive Systems Conference (DIS '19)*. Association for Computing Machinery, New York, NY, USA, 147–160. https://doi.org/10.1145/3322276.3323694

[22] Audrey Desjardins, Timea Tihanyi, Freesoul El Shabazz-Thompson, Brock Craft, and Julia Saimo. 2023. THE INNER EAR: CAPTURING AND PHYSICALIZING HOME VIBRATIONS. In *Proceedings of the 2023 ACM Designing Interactive Systems Conference (DIS '23)*. Association for Computing Machinery, New York, NY, USA, 594–607. https://doi.org/10.1145/3563657.3596070

[23] Laura Devendorf, Leah Buechley, Noura Howell, Jennifer Jacobs, Cindy Hsin-Liu Kao, Martin Murer, Daniela Rosner, Nica Ross, Robert Soden, Jared Tso, and Clement Zheng. 2023. Towards Mutual Benefit: Reflecting on Artist Residencies as a Method for Collaboration in DIS. In *Designing Interactive Systems Conference*. ACM, Pittsburgh PA USA, 124–126. https://doi.org/10.1145/3563703.3591452

[24] Paul L. DiMatteo. 1976. Method of generating and constructing three-dimensional bodies. https://patents.google.com/patent/US3932923A/en

[25] Shelby Doyle, Erin Hunt, and Kelly Devitt. 2018. WAFT. In *Proceedings of the 37th Annual Conference of the Association for Computer Aided Design in Architecture (ACADIA)*. Mexico City, Mexico.

[26] Chad Duty, Christine Ajinjeru, Vidya Kishore, Brett Compton, Nadim Hmeidat, Xun Chen, Peng Liu, Ahmed Arabi Hassen, John Lindahl, and Vlastimil Kunc. 2018. What makes a material printable? A viscoelastic model for extrusion-based 3D printing of polymers. *Journal of Manufacturing Processes* 35 (Oct. 2018), 526–537. https://doi.org/10.1016/j.jmapro.2018.08.008

[27] Pam East. 2007. *Enameling on Metal Clay*. Kalmbach Books.

[28] Eazao. 2022. Eazao Zero - Eazao. https://www.eazao.com/product/eazao-zero/

[29] Alliance for Metal Clay Arts Worldwide (AMCAW). 2018. A Brief History of Metal Clay. https://amcaw.org/learning-center/a-brief-history-of-metal-clay/

[30] Alliance for Metal Clay Arts Worldwide (AMCAW). 2018. Metal Clay Firing Methods and Equipment. https://amcaw.org/learning-center/metal-clay-firing-methods-and-equipment/

[31] Alliance for Metal Clay Arts Worldwidew. 2018. Alliance for Metal Clay Arts Worldwide - Welcome to AMCAW! https://amcaw.org/

[32] Jack Forman, Mustafa Doga Dogan, Hamilton Forsythe, and Hiroshi Ishii. 2020. DefeXtiles: 3D Printing Quasi-Woven Fabric via Under-Extrusion. In *Proceedings of the 33rd Annual ACM Symposium on User Interface Software and Technology*. Association for Computing Machinery, New York, NY, USA, 1222–1233. http://doi.org/10.1145/3379337.3415876

[33] Frikk H Fossdal, Vinh Nguyen, Rogardt Heldal, Corie L. Cobb, and Nadya Peek. 2023. Vespidae: A Programming Framework for Developing Digital Fabrication Workflows. In *Proceedings of the 2023 ACM Designing Interactive Systems Conference (DIS '23)*. Association for Computing Machinery, New York, NY, USA, 2034–2049. https://doi.org/10.1145/3563657.3596106

[34] Virtual Foundry. 2023. Bound Metal 3D Printing for the Lab, Classroom or Studio. https://thevirtualfoundry.com/

[35] Randall M. German. 2016. Sintering Trajectories: Description on How Density, Surface Area, and Grain Size Change. *JOM* 68, 3 (March 2016), 878–884. https://doi.org/10.1007/s11837-015-1795-8

[36] Michael Golub. 2017. *Characterization of Tensile and Hardness Properties and Microstructure of 3D Printed Bronze Metal Clay*. M.S.M.E. Purdue University, United States – Indiana. http://www.proquest.com/docview/1980720465/abstract/5CA88D3157224A5APQ/1 ISBN: 9780355306385.

[37] Joamin Gonzalez-Gutierrez, Santiago Cano, Stephan Schuschnigg, Christian Kukla, Janak Sapkota, and Clemens Holzer. 2018. Additive Manufacturing of Metallic and Ceramic Components by the Material Extrusion of Highly-Filled Polymers: A Review and Future Perspectives. *Materials* 11, 5 (May 2018), 840. https://doi.org/10.3390/ma11050840 Number: 5 Publisher: Multidisciplinary Digital Publishing Institute.

[38] W. B. Harris. 1957. *HEALTH AND SAFETY IN POWDER METAL HANDLING*. Technical Report NYO-4869. New York Operations Office. Health and Safety Lab., AEC. https://doi.org/10.2172/4350771

[39] Sue Heaser. 2012. *Metal Clay for Jewelry Makers: The Complete Technique Guide by Heaser, Sue* (1st edition ed.). Delphi Glass, Loveland, CO.

[40] Sue Heaser. 2021. *Magical Metal Clay: Amazingly Simple No-Kiln Techniques for Making Beautiful Accessories*. David & Charles.

[41] Jean Hergel, Kevin Hinz, Sylvain Lefebvre, and Bernhard Thomaszewski. 2019. Extrusion-based ceramics printing with strictly-continuous deposition. *ACM Transactions on Graphics* 38, 6 (Nov. 2019), 194:1–194:11. https://doi.org/10.1145/3355089.3356509

[42] Juichi Hirasawa and Shinji Otani. 1996. Precious Metal Clay. https://patents.google.com/patent/JPH083662A

[43] Brandon Holschuh. 2009. *The Jeweler's Studio Handbook: Traditional and Contemporary Techniques for Working with Metal and Mixed Media Materials*. Quarry Books.

[44] Ryan Hoover. 2023. Xylinus. http://www.ryanhoover.org/rd/xylinus.php

[45] ISO/ASTM. 2023. ISO/ASTM standard 52900. https://www.astm.org/f3177-21.html

[46] Hadar Jacobson. 2008. *The Handbook of Metal Clay: Textures and Forms* (1 ed.). Hadar's Clay. https://store.artinsilver.com/cobhaofmeclt.html

[47] Hadar Jacobson. 2023. Hadar's Clay™. https://store.artinsilver.com/purchasepmc.html

[48] Barbara Katzbauer. 1998. Properties and applications of xanthan gum. *Polymer Degradation and Stability* 59, 1 (Jan. 1998), 81–84. https://doi.org/10.1016/S0141-3910(97)00180-8

[49] Jonathan Keep. 2022. digital 3D ceramic printing journal. http://www.keep-art.co.uk/journal_1.html

[50] Ahmet Çağrı Kılınç, Ali Aydın Goktas, Özgür Yasin Keskin, and Serhan Köktaş. 2021. Extrusion-Based 3D Printing of CuSn10 Bronze Parts: Production and Characterization. *Metals* 11, 11 (Nov. 2021), 1774. https://doi.org/10.3390/met11111774 Number: 11 Publisher: Multidisciplinary Digital Publishing Institute.

[51] Eldy S. Lazaro Vasquez, Netta Ofer, Shanel Wu, Mary Etta West, Mirela Alistar, and Laura Devendorf. 2022. Exploring Biofoam as a Material for Tangible Interaction. In *Designing Interactive Systems Conference*. ACM, Virtual Event Australia, 1525–1539. https://doi.org/10.1145/3532106.3533494

[52] Alain Le-Bail, Bianca Chieregato Maniglia, and Patricia Le-Bail. 2020. Recent advances and future perspective in additive manufacturing of foods based on 3D printing. *Current Opinion in Food Science* 35 (Oct. 2020), 54–64. https://doi.org/10.1016/j.cofs.2020.01.009

[53] Anastasios Lekkas, Andreas R. Dahl, Morten Breivik, and Thor I. Fossen. 2013. Continuous-Curvature Path Generation using Fermat's Spiral. *183-198* (2013). https://doi.org/10.4173/mic.2013.4.3 Accepted: 2017-11-07T08:34:58Z Publisher: Norsk Forening for Automatisering.

[54] Jia Ping Li, Joost R. de Wijn, Clemens A. Van Blitterswijk, and Klaas de Groot. 2006. Porous Ti6Al4V scaffold directly fabricating by rapid prototyping: Preparation and in vitro experiment. *Biomaterials* 27, 8 (March 2006), 1223–1235. https://doi.org/10.1016/j.biomaterials.2005.08.033

[55] Jeffrey I. Lipton and Hod Lipson. 2016. 3D Printing Variable Stiffness Foams Using Viscous Thread Instability. *Scientific Reports* 6, 1 (Aug. 2016), 29996. https://doi.org/10.1038/srep29996 Number: 1 Publisher: Nature Publishing Group.

[56] Rubén Lostado-Lorza, Marina Corral-Bobadilla, Saúl Iñiguez-Macedo, Fátima Somovilla-Gómez, and Celia Sabando-Fraile. 2023. Tensile strength, elastic modulus and thermal conductivity of 3D-Printed components using bronze/PLA filament. In *2023 8th International Conference on Smart and Sustainable Technologies (SpliTech)*. 1–5. https://doi.org/10.23919/SpliTech58164.2023.10193626

[57] Tim McCreight. 1994. *Practical Casting: A Studio Reference, Revised Edition* (2nd edition ed.). Brynmorgen Press.

[58] Abhishek Mehta, Le Zhou, Holden Hyer, Thinh Huynh, Binghao Lu, Kevin Graydon, Erica J. Drobner, Sun Hong Park, and Yongho Sohn. 2022. Microstructural characteristics and mechanical properties of additively manufactured Cu–10Sn alloys by laser powder bed fusion. *Materials Science and Engineering: A* 838 (March 2022), 142775. https://doi.org/10.1016/j.msea.2022.142775

[59] David Mellis, Sean Follmer, Björn Hartmann, Leah Buechley, and Mark D. Gross. 2013. FAB at CHI: digital fabrication tools, design, and community. In *CHI '13 Extended Abstracts on Human Factors in Computing Systems (CHI EA '13)*. ACM, New York, NY, USA, 3307–3310. https://doi.org/10.1145/2468356.2479673

[60] Desktop Metal. 2023. Deep Dive: Bound Metal Deposition (BMD). https://www.desktopmetal.com/resources/deep-dive-bmd

[61] Desktop Metal. 2023. Studio System™. https://www.desktopmetal.com/products/studio

[62] One Click Metal. 2023. One Click Metal: The system solution for metal 3D printing. https://oneclickmetal.com/

[63] Pauline L. Nasatto, Frédéric Pignon, Joana L. M. Silveira, Maria Eugênia R. Duarte, Miguel D. Noseda, and Marguerite Rinaudo. 2015. Methylcellulose, a Cellulose Derivative with Original Physical Properties and Extended Applications. *Polymers* 7, 5 (May 2015), 777–803. https://doi.org/10.3390/polym7050777 Number: 5 Publisher: Multidisciplinary Digital Publishing Institute.

[64] Taylor V. Neumann and Michael D. Dickey. 2020. Liquid Metal Direct Write and 3D Printing: A Review. *Advanced Materials Technologies* 5, 9 (2020), 2000070. https://doi.org/10.1002/admt.202000070 _eprint: https://onlinelibrary.wiley.com/doi/pdf/10.1002/admt.202000070.

[65] Jifei Ou, Chin-Yi Cheng, Liang Zhou, Gershon Dublon, and Hiroshi Ishii. 2015. Methods of 3D Printing Micro-pillar Structures on Surfaces. In *Adjunct Proceedings of the 28th Annual ACM Symposium on User Interface Software & Technology (UIST '15 Adjunct)*. Association for Computing Machinery, New York, NY, USA, 59–60. https://doi.org/10.1145/2815585.2817812

[66] Chinnapat Panwisawas, Yuanbo T. Tang, and Roger C. Reed. 2020. Metal 3D printing as a disruptive technology for superalloys. *Nature Communications* 11, 1 (May 2020), 2327. https://doi.org/10.1038/s41467-020-16188-7 Number: 1 Publisher: Nature Publishing Group.

[67] Erwin Peng, Danwei Zhang, and Jun Ding. 2018. Ceramic Robocasting: Recent Achievements, Potential, and Future Developments. *Advanced Materials* 30, 47 (2018), 1802404. https://doi.org/10.1002/adma.201802404 _eprint: https://onlinelibrary.wiley.com/doi/pdf/10.1002/adma.201802404.

[68] Ronald Rael and Virginia San Fratello. 2018. *Printing Architecture: Innovative Recipes for 3D Printing*. Princeton Architectural Press, Hudson, New York.

[69] Ronald Rael, Virginia San Fratello, and Phirak Suon. [n. d.]. Bad Ombres v.2 | Emerging Objects. http://www.emergingobjects.com/project/bad-ombres-v-2/

[70] Baker Ralph. 1925. Method of making decorative articles. https://patents.google.com/patent/US1533300A/en

[71] Kedarnath Rane, Kevin Castelli, and Matteo Strano. 2019. Rapid surface quality assessment of green 3D printed metal-binder parts. *Journal of Manufacturing Processes* 38 (Feb. 2019), 290–297. https://doi.org/10.1016/j.jmapro.2019.01.032

[72] Kedarnath Rane and Matteo Strano. 2019. A comprehensive review of extrusion-based additive manufacturing processes for rapid production of metallic and

ceramic parts. *Advances in Manufacturing* 7, 2 (June 2019), 155–173. https://doi.org/10.1007/s40436-019-00253-6

[73] Michael L. Rivera, S. Sandra Bae, and Scott E. Hudson. 2023. Designing a Sustainable Material for 3D Printing with Spent Coffee Grounds. In *Proceedings of the 2023 ACM Designing Interactive Systems Conference (DIS '23)*. Association for Computing Machinery, New York, NY, USA, 294–311. https://doi.org/10.1145/3563657.3595983

[74] Oleg V. Roman and Henry H. Hausner. 1962. Investigation in the Linear Shrinkage of Metal Powder Compacts During Sintering. *Scientific Principles of Powder Metallurgy* 9, 6 (1962), 228–236. https://doi.org/10.2497/jjspm.9.228

[75] Eva Sanchez-Rexach, Trevor G. Johnston, Coralie Jehanno, Haritz Sardon, and Alshakim Nelson. 2020. Sustainable Materials and Chemical Processes for Additive Manufacturing. *Chemistry of Materials* 32, 17 (Sept. 2020), 7105–7119. https://doi.org/10.1021/acs.chemmater.0c02008 Publisher: American Chemical Society.

[76] MilliporeSigma (SigmaAldrich). 2023. Bronze Powder SDS. https://www.sigmaaldrich.com/US/en/substance/bronze1234598765

[77] Rio Grande Jewelry Supply. 2021. Metal Clay - Rio Grande. https://www.riogrande.com/product/metals/metal-clay/

[78] Rio Grande Jewelry Supply. 2022. BRONZclay SDS. https://www.riogrande.com/knowledge-hub/safety-data-sheets/101010-sds/

[79] Haruki Takahashi and Homei Miyashita. 2017. Expressive Fused Deposition Modeling by Controlling Extruder Height and Extrusion Amount. In *Proceedings of the 2017 CHI Conference on Human Factors in Computing Systems*. ACM, Denver Colorado USA, 5065–5074. https://doi.org/10.1145/3025453.3025933

[80] Engineering Toolbox. 2004. Metals and Alloys - Densities. https://www.engineeringtoolbox.com/metal-alloys-densities-d_50.html

[81] OAR US EPA. 2016. Health and Environmental Effects of Particulate Matter (PM). https://www.epa.gov/pm-pollution/health-and-environmental-effects-particulate-matter-pm

[82] Metal Powders USA. [n. d.]. Bronze Powder SDS. https://0201.nccdn.net/1_2/000/000/119/673/msds_bronze-2019.pdf

[83] Metal Powders USA. 2023. Certificates of Analysis. https://metalpowdersusa.com/cofa-and-sds

[84] Abel Vincze. [n. d.]. Involute spur gear generator and simulator. https://geargenerator.com/

[85] Alexander Watson, John Belding, and Brett D. Ellis. 2020. Characterization of 17-4 PH Processed via Bound Metal Deposition (BMD). In *TMS 2020 149th Annual Meeting & Exhibition Supplemental Proceedings (The Minerals, Metals & Materials Series)*. Springer International Publishing, Cham, 205–216. https://doi.org/10.1007/978-3-030-36296-6_19

[86] Xueying Wei, Ingolf Behm, Tony Winkler, Stefan Scharf, Xujun Li, and Rüdiger Bähr. 2022. Experimental Study on Metal Parts under Variable 3D Printing and Sintering Orientations Using Bronze/PLA Hybrid Filament Coupled with Fused Filament Fabrication. *Materials* 15, 15 (Jan. 2022), 5333. https://doi.org/10.3390/ma15155333 Number: 15 Publisher: Multidisciplinary Digital Publishing Institute.

[87] Eric W. Weisstein. [n. d.]. Rose Curve. https://mathworld.wolfram.com/ Publisher: Wolfram Research, Inc..

[88] CeCe Wire. 2007. *Creative Metal Clay Jewelry: Techniques, Projects, Inspiration* (1st edition ed.). Lark Crafts.

[89] Terry Wohlers. 2017. Desktop Metal targets speed, cost and high-volume production AM. *Metal AM magazine* 3, 2 (2017). https://www.metal-am.com/articles/desktop-metal-targets-speed-cost-and-high-volume-production-3d-printing/

[90] Marco Zago, Nora Francesca Maria Lecis, Maurizio Vedani, and Ilaria Cristofolini. 2021. Dimensional and geometrical precision of parts produced by binder jetting process as affected by the anisotropic shrinkage on sintering. *Additive Manufacturing* 43 (July 2021), 102007. https://doi.org/10.1016/j.addma.2021.102007

[91] Haisen Zhao, Fanglin Gu, Qi-Xing Huang, Jorge Garcia, Yong Chen, Changhe Tu, Bedrich Benes, Hao Zhang, Daniel Cohen-Or, and Baoquan Chen. 2016. Connected fermat spirals for layered fabrication. *ACM Transactions on Graphics* 35, 4 (July 2016), 1–10. https://doi.org/10.1145/2897824.2925958

[92] L. Zhong, M. Oostrom, M. J. Truex, V. R. Vermeul, and J. E. Szecsody. 2013. Rheological behavior of xanthan gum solution related to shear thinning fluid delivery for subsurface remediation. *Journal of Hazardous Materials* 244-245 (Jan. 2013), 160–170. https://doi.org/10.1016/j.jhazmat.2012.11.028

[93] H H Zhu, L Lu, and J Y H Fuh. 2006. Study on Shrinkage Behaviour of Direct Laser Sintering Metallic Powder. *Proceedings of the Institution of Mechanical Engineers, Part B: Journal of Engineering Manufacture* 220, 2 (Feb. 2006), 183–190. https://doi.org/10.1243/095440505X32995 Publisher: IMECHE.

[94] Amit Zoran and Leah Buechley. 2013. Hybrid Reassemblage: An Exploration of Craft, Digital Fabrication and Artifact Uniqueness. *Leonardo* 46, 1 (Feb. 2013), 4–10. https://doi.org/10.1162/LEON_a_00477